ADVANCED ENERGY MATERIALS
www.advenergymat.de

A Three Dimensional Multi-Layered Sliding Triboelectric Nanogenerator

Weiming Du, Xun Han, Long Lin, Mengxiao Chen, Xiaoyi Li, Caofeng Pan, and Zhong Lin Wang**

Harvesting new renewable energy from ambient environment has attracted lots of interest not only for searching renewable and "green" energy for sustainable development, but also for achieving self-powered nanosystems at a small scale.[1] Until now, various energies have been harvested, such as solar,[2] geothermal,[3] biomass,[4] tide,[5] and wind.[6] As one of the most common energy in our living environment, mechanical energy has also been scavenged with diverse approaches based on piezoelectrics,[7] electrostatics,[8] and electromagnetics.[9] Recently, a triboelectric nanogenerator (TENG) has been demonstrated to be an effective way to convert mechanical energy into electricity,[10] with performance depending on the coupling of triboelectrification[11] and electrostatic induction.[10a] Among the factors that affect the performance of the TENG, the sufficient charge separation[12] and the friction area[13] are the two key factors. For charge separation, it depends on the materials used in the device and we can choose materials (one easy to gain electrons, and the other easy to lose electrons) to increase the output performance.[14] For the friction area, compared with increasing the size of the device, it is a better choice to extend the device from a 2D planar device[15] to a 3D device.

Here, we develop 3D-TENG, with layer-by-layer stacked polyvinyl chloride (PVC) and aluminum as friction materials, based on an in-plane sliding mode between every two adjacent surfaces. Such a 3D multi-layered structure largely increases the friction area in the same space that contributes to the increase in the transferred charge quantity in the circuit. For a 3D-TENG consisting of 20 layers of PVC and 20 layers of aluminum as friction films, the open-circuit voltage (V_{oc}) reaches 800 V, the peak short-circuit current density (J_{sc}) of 5.5 mA m^{-2} and a peak power density of 4.4 W m^{-2}, a maxiumum charge transfer quantity of 2.6 μC, with a sliding displacement of 15 mm. The results clearly demonstrate that the transferred charge quantity monotonically increases with increasing numbers of friction layers. Furthermore, the transferred charge quantity has a good linear relationship with the sliding displacement in a range of 3–15 mm, which means that 3D-TENG can be used as a self-powered displacement sensor. 160 commercial light-emitting diode (LED) bulbs are instantaneously lit up because the output power of the 3D-TENG is very high; additionally the power generated by the 3D-TENG can be easily and effectively stored into an energy storage device such as a capacitor. The 3D-TENG takes full advantage of the space and largely improves the output of the TENGs, with great potential in self-powered systems, environmental monitoring, defense technology, and even personal electronics.

The basic structure of the 3D-TENG is composed of PVC and aluminum friction films stacking layer-by-layer, as illustrated in **Figure 1**a. The digital image of the fabricated device is presented in Figure 1b. To demonstrate the principle of the device, it is made of 20 layers of PVC and 20 layers of aluminum. Comparing to the previously reported devices,[16] such 3D-TENG has two advantages. First, it can increase the friction area tens of times compared to the former TENG. Second, since the 3D-TENG can be treated as a large number of individual planar TENGs connected in parallel, it can largely enhance the output current of the device. Nanowires are formed on the surface of PVC films by an inductively coupled plasma (ICP) method (Figure 1c) to increase the friction area[17] so the output of the device is expected to be improved. A 30°-tilted view scanning electron microscopy (SEM) image of the nanostructured PVC surface is shown in Figure 1d, and a higher magnification SEM image is presented as an inset. It is obvious that the PVC nanowires are uniformly distributed on the PVC surface with an average diameter of 100–200 nm and an average length of 500 nm, respectively.

The working principle of the 3D-TENG is schematically depicted in **Figure 2**a–e step by step. For easily understanding, we note that the PVC and aluminum films fully contacted with each other as the original position (Figure 2a). At the original position, the PVC and aluminum films are fully overlapped. When the PVC films slide apart from and rub the aluminum films (Figure 2b), the electrons transfer from the aluminum to the PVC because PVC easily gains electrons while aluminum easily loses electrons, according to the triboelectric series.[18] The electrons transferred to the PVC films will only distribute in the surface of PVC films and will not leak out for an extended period of time. At the same time, the separation causes a higher electric potential at the aluminum films, which will drive current flow from the electrode of PVC films to the aluminum film in order to generate an electric potential drop that cancels the tribo-charge-induced potential. The current flow continues in the whole separation process until they are

W. Du, X. Han, M. Chen, X. Li, Prof. C. F. Pan, Prof. Z. L. Wang
Beijing Institute of Nanoenergy and Nanosystems
Chinese Academy of Sciences
Beijing 100083, China
E-mail: cfpan@binn.cas.cn; zlwang@gatech.edu
L. Lin, Prof. Z. L. Wang
School of Materials Science and Engineering
Georgia Institute of Technology
Atlanta, GA 30332–0245, USA

DOI: 10.1002/aenm.201301592

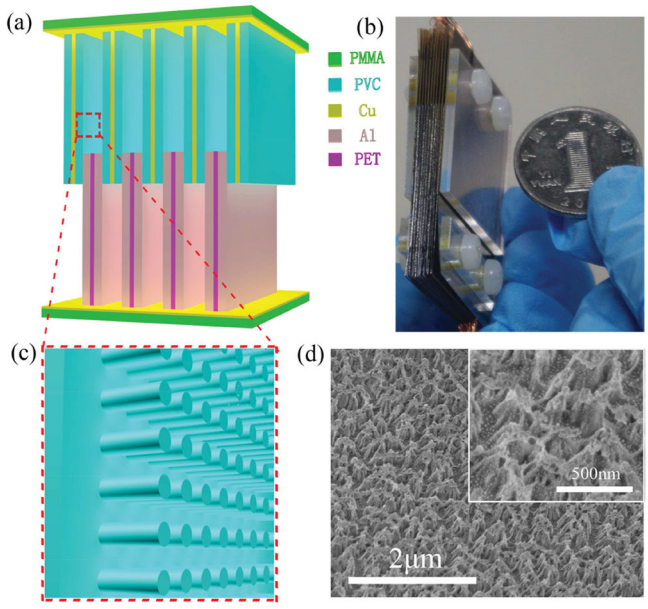

Figure 1. Schematic illustration, digital and electron microscopic images of a 3D-TENG. a) Schematic structure and b) digital image of a fabricated 3D-TENG. c) Magnified schematic and d) SEM image of nanowires structured PVC films at the tilted view of 30°. The inset in (d) is an enlarged SEM image showing the details of the PVC nanostructured surface.

fully separated (Figure 2c), and the V_{oc} reaches its maximum. Subsequently, as the PVC films slide back, the PVC films begin to come into contact with aluminun films and cause the electric potential at the aluminum to be lower than the electrode of the PVC films. As a consequence, the electrons will flow back in the opposite direction from aluminum films to the electrode of PVC films (Figure 2d). This process continues until the PVC and aluminum films are overlapped again (Figure 2e). This is a full cycle of electrical energy generation, and the periodic AC output generated due to the cyclic motion of the device.

According to a previous study,[19] the theoretical V_{oc} of a conductor-to-dielectric sliding-mode TENG is given by:

$$V_{oc} = \frac{\sigma x}{\varepsilon_0 (l - x)} \frac{d}{\varepsilon_r} \quad (1)$$

where σ is the transferred charge density for the non-overlapped region, x is the consecutive sliding displacement, l is the geometric size of the PVC and aluminum film in longitudinal direction, d and ε_r are the thickness and the relative dielectric constant of PVC film, respectively. With a consecutive sliding displacement of 15 mm, a length of 20 mm, thickness of 0.1 mm and transferred charge density of 110 μC m^{-2}, which is the measured value of the device in Figure 2b, the maximum theoretical V_{oc} can reach 2663.4 V based on Equation (1).

A finite element simulation was carried out to illustrate the electrostatic potential difference between the two electrodes at the consecutive sliding displacement of 15 mm (Figure 2f). The model presented here has 20 layers of PVC and 20 layers of aluminum and friction area is 35 mm × 15 mm of each layer, which is the same as the devices we measured in this work. All of the PVC and aluminum films are in close contact with each other. The PVC and aluminum are initially assigned with a charge density of –110 μC m^{-2} and 110 μC m^{-2}, respectively. The electric potential difference between the two electrodes at a consecutive sliding displacement of 15 mm can reach 1.37 × 10^6 V in an ideal case.

The electrical output of the 3D-TENG was measured with a linear motor (Linmot E1100). The maximum consecutive sliding displacement is 15 mm. The friction films slide with a symmetric acceleration rate of ±20 m s^{-2} and a maximum speed of 0.55 m s^{-1}. The V_{oc} and transferred charge quantity ($\triangle Q$) were measured by an electrometer (Keithley 6514). At a consecutive sliding displacement of 15 mm, the V_{oc} reaches ≈800 V (**Figure 3**a), and the transferred charge quantity with a maximum density of ≈115 μC m^{-2}, as shown in Figure 3b, which is higher than the previous work. As a result, the totally transferred charge quantity reaches 2.6 μC, which is much higher than the values for planar TENGs[15,20] due to the increasing of the friction area when the device extends to 3D structure. The short-circuit current (I_{sc}) was measured by a current preamplifier (Stanford Research Systems SR570) and J_{sc} is around 5.5 mA m^{-2} (Figure 3c). This AC output can be rectified to DC output by a full-wave rectifier bridge (Figure 3d).

The relationship between the output of the 3D-TENG and the number of friction layers is also systematically investigated. It

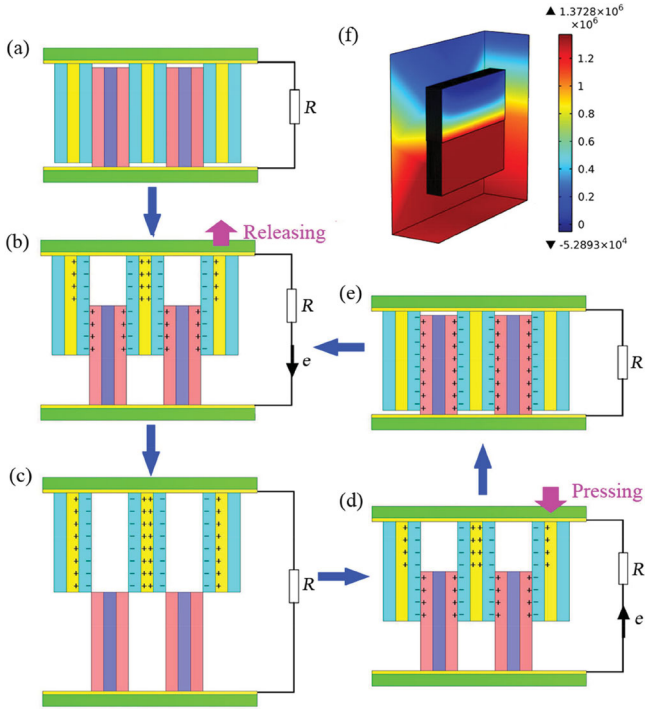

Figure 2. Working mechanism of the 3D-TENG. a) The original state with the PVC and aluminum films fully overlapped and closely contacted. b) PVC films sliding and separating with the aluminum films causes a higher electric potential at the aluminum films, which drives the electrons through the external circuit. c) A full separation of the 3D-TENG at a consecutive sliding displacement of 15 mm. d) PVC films sliding back and driving the electrons back to the PVC films. e) The entirely contacting state of the 3D-TENG. f) Finite element simulation of the electric potential of the 3D-TENG at consecutive sliding displacement of 15mm.

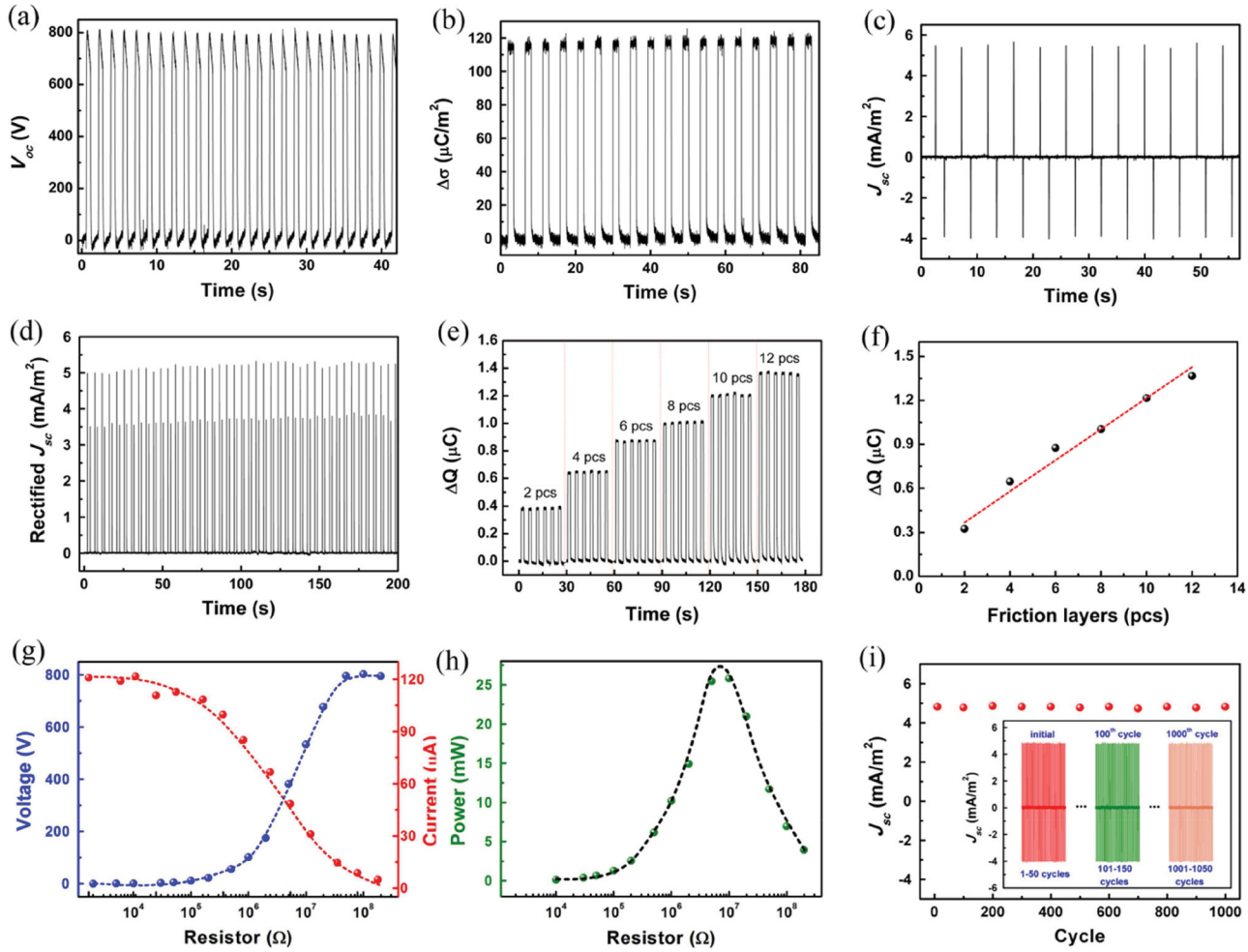

Figure 3. Electric output of a 3D-TENG with 40 layers friction films. a) The open-circuit voltage (V_{oc}), b) the transferred charge density ($\triangle\sigma$), c) the short-circuit current density (J_{sc}), and d) the rectified short-circuit current density of the fabricated 3D-TENG with a sliding displacement of 15 mm and symmetric acceleration rate of ±20 m s^{-2}. e) The measured transferred charge quantity ($\triangle Q$) with different number of friction layers. f) The summarized relationship between the transferred charge quantity and the number of friction layers. g) The relationship between the output voltage/current and the resistance of the external load. h) The relationship between the power and the resistance of the external load. The maximum power is received ≈27 mW when the external load is 8 MΩ. i) The current output stability of the device within 1000 cycles.

is obvious that the output of the 3D-TENG effectively increases with the increase in friction layers, as shown in Figure 3e. The transferred charge quantity increases from 0.4 to 1.37 μC when the number of friction layers increases from 2 to 12. Figure 3f shows that the transferred charge quantity increases linearly with the number of friction layers. However, we still can find that part of the charge gets lost during the transport process, and it is not strictly doubled when the friction layers increase from 2 to 4. This may be due to the in-series resistance caused by the integration process; the performance of the 3D-TENG can be further enhanced by optimizing the design and decreasing this in-series resistance.

The power output capability of the 3D-TENG was investigated by using resistors as external loads. As shown in Figure 3g, the output voltage increases quickly as the resistance increases from 1MΩ to 100 MΩ, and then saturates when the resistance further increases. The output current follows a reverse trend when compared to the output voltage. As a result, the output power is maximized at ≈27 mW when the external load with a resistance of ≈8 MΩ, which is shown in Figure 3h. The stability of the performance has also been measured. The result shows that the output of the device remains very stable after 1000 cycles, as shown in Figure 3i.

The output of the 3D-TENG also depends on measurement conditions, such as the maximum consecutive sliding displacement and the velocity. A systematic study of the relationship between the V_{oc} and the consecutive sliding displacement was carried out experimentally, as shown in **Figure 4**a. The transferred charge quantities are about 0.143, 0.609, 1.275, 2.005, and 2.579 μC when the consecutive sliding displacements are 3, 6, 9, 12, and 15 mm, respectively. After extracting the charge transfer values from Figure 4a and plotting in Figure 4b, this shows that the transferred charge quantity has a linear relationship with the consecutive sliding displacement. This means that the 3D-TENG can be used as a self-powered displacement sensor. The relationship between the I_{sc} and the sliding velocity

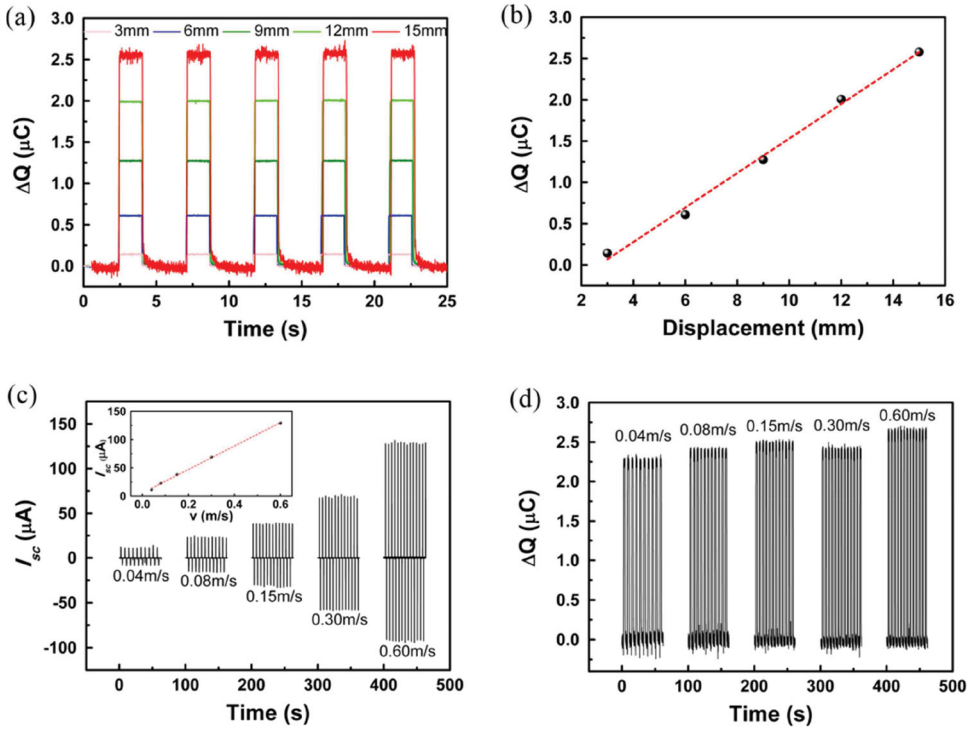

Figure 4. The electrical output of a 3D-TENG depends on the sliding displacement and measuring velocity. a) The measured transferred charge quantities ($\triangle Q$) at five different sliding displacements: 3, 6, 9, 12, and 15 mm, respectively. b) The relationship between the transferred charge quantity and the sliding displacement, showing that they have a good linear relationship. c) The measured short-circuit currents at five different sliding velocities of 0.04, 0.08, 0.15, 0.30, and 0.60 m s^{-1}, respectively. The output current increases with increasing the sliding velocity. The inset shows the relationship between the short-circuit current and the sliding velocity, which also have a good linear relationship. d) The transferred charge quantities measured at five different sliding velocities of 0.04, 0.08, 0.15, 0.30, and 0.60 m s^{-1}; the transferred charge quantity remains the same at different sliding velocities.

is shown in Figure 4c. The I_{sc} is measured at different sliding velocities of 0.04, 0.08, 0.15, 0.30, and 0.60 m s^{-1}, and the corresponding output short-circuit currents are 11.1, 22.9, 38.3, 68.9, and 129.2 μA. The inset figure shows that the I_{sc} increases with the increasing of the sliding velocity, and follows a good linear relationship. Consequently, the device has a great potential application as a self-powered velocity sensor. In contrast, the sliding velocity almost has no influence on the transferred charge quantity, which is only determined by the sliding displacement when the device is fabricated (Figure 4d).

The 3D-TENG can be directly used as a power source to drive continuum-electricity-consuming personal electric devices due to its high output. When the PVC films slide apart from the aluminum films at a symmetric acceleration rate of ±20 m s^{-2} and a maximum speed of 0.55 m s^{-1}, 160 green LED bulbs are lit instantly. **Figure 5**a,b show the dark and lighting-up states of the LED bulbs. On the other hand, for most of the self-powered sensors, the devices usually work with a very short active mode and then stay in a long sleep mode. Then, the energy harvested by the 3D-TENG during the sleep mode can be rectified and stored in an energy storage device, such as a battery or capacitor, and can then power the device in the active mode for sensing, data processing, and wireless signal transmission. As shown in Figure 5c, the 3D-TENG is used to charge two 3.3 and 22 μF capacitors. It takes ≈36 cycles to charge the capacitor to 68 V for the 3.3 μF one, and to 17 V for the 22 μF capacitor. Figure 5d depicts each charge cycle of the charge process. The capacitor is charged twice within each cycle, corresponding to the two output peaks during a pressing/releasing cycle of a 3D-TENG, as shown in the inset of Figure 5d.

In summary, we have demonstrated a novel design of a 3D-TENG with multi-layered structure. It not only largely increases the transferred charge quantity owning to the increasing of the friction area in the same space, but also largely improves the output current by connecting all the TENGs in parallel. By converting the mechanical energy in the sliding motion of 15 mm, the 3D-TENG delivers an open-circuit voltage of 800 V and a short-circuit current density of 5.5 mA m^{-2} with the maximum instantaneous power density of 4.4 W m^{-2}. The transfered charge quantity increases linearly with the number of friction layers, reaching about 2.6 μC for a 40 layers 3D-TENG, proving that the 3D extension is an effective way to improve the output of TENGs. A linear relationship is obtained between the transferred charge quantity and the sliding displacement, and it also exists between I_{sc} and the sliding velocity, which enables its application as a self-powered displacement and velocity sensor. Due to its high output power, the power generated by the 3D-TENG can be used to light up 160 commercial LED bulbs instantaneously, and it can also be easily and effectively stored into energy storage device such as a capacitor. The 3D-TENG opens up a new field of the 3D device,

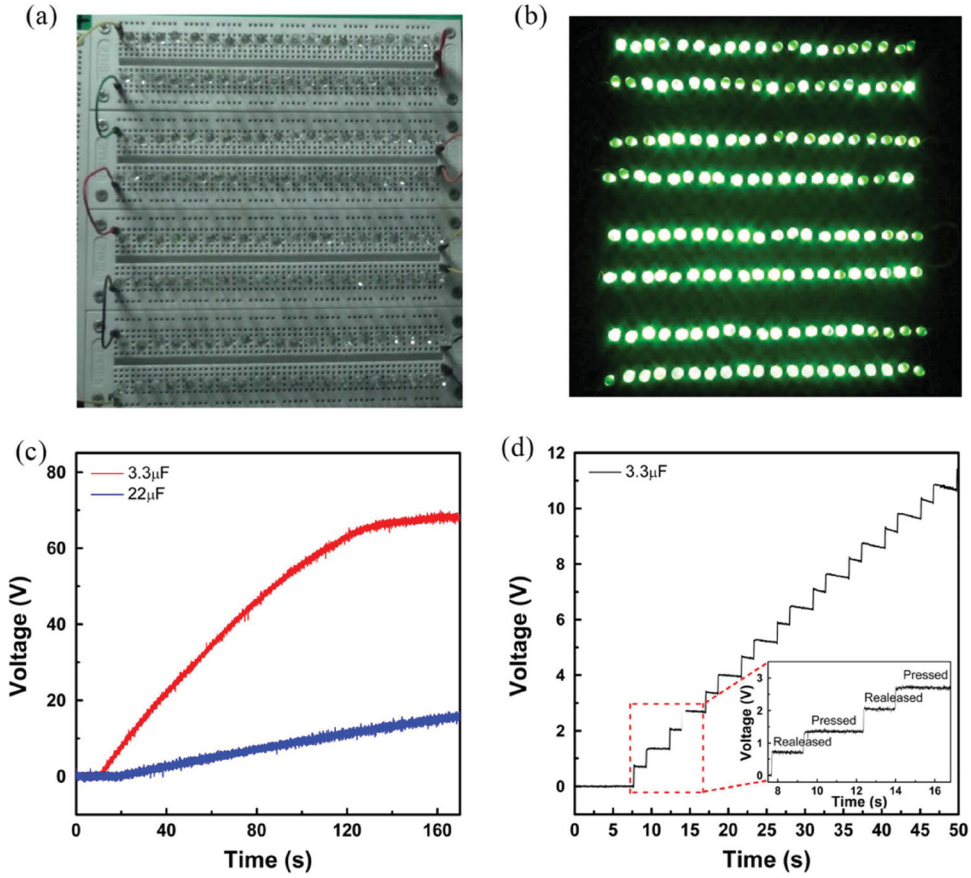

Figure 5. The application of the 3D-TENG. The dark (a) and lit up (b) states of 160 green LED bulbs driven simultaneously by the fabricated 3D-TENG. c) The charging curve of a 3.3 μF and a 22 μF capacitances, which are charged by the 3D-TENG. d) The charging circles of the 3.3 μF capacitance, clearly showing the charging process.

which may have practical applications in havesting mechanical energy because of the largely improved output of the TENGs.

Experimental Section

Fabrication of Nanowire Array on the Surface of the PVC Film: 0.1 mm thick PVC films were cleaned with alcohol, isopropyl alcohol, and deionized water in sequence, and then blown dry with compressed air. Subsequently, a layer of gold particles with diameters around 10 nm was sputtered onto PVC films as the mask. Then an ICP process was used to fabricate aligned nanowires on the surface of PVC films for 40 s. Ar and O_2 gases were introduced into the ICP chamber with the flow of 5.0 and 55.0 sccm, respectively. One power source of 440 W was used to generate a large density of plasma, and the other power of 100 W was used to accelerate the plasma ions. The SEM image of the nanostructured PVC films was taken by Hitach S-5500.

The Fabrication of a 3D-TENG with 20 Layers of Al Films and 20 Layers of PVC Films: 10 pieces of PET films (substrate) (35 mm × 45 mm) with a thickness of 0.1 mm were cleaned and then deposited with a 100 nm layer of aluminum on both of the two sides. 20 pieces of PVC thin films (35 mm × 45 mm) with a thickness of 0.1 mm were cleaned and deposited with 100 nm of copper on one side of the film by magnetron sputtering. Then all of the Al and PVC films were stacked layer-by-layer, with every aluminum layer contacting two PVC layers on both sides, and every PVC layer contacting two aluminum layers on both sides as well, as shown in Figure 1a. All electrodes on the PVC films were connected in parallel, and all the aluminum films were connected in parallel.

Acknowledgements

W.D. and X.H. contributed equally to this work. This research was supported by the "thousands talents" program for pioneer researcher and his innovation team, China, and the Knowledge Innovation Program of the Chinese Academy of Science (Grant No. KJCX2-YW-M13).

Received: October 18, 2013
Revised: February 12, 2014
Published online:

[1] a) Z. L. Wang, J. H. Song, *Science* **2006**, *312*, 242; b) Z. L. Wang, *Adv. Funct. Mater.* **2008**, *18*, 3553; c) Z. L. Wang, *Nano Res.* **2008**, *1*, 1; d) Z. L. Wang, *Sci. Am.* **2008**, *298*, 82; e) Z. L. Wang, G. Zhu, Y. Yang, S. H. Wang, C. F. Pan, *Mater. Today* **2012**, *15*, 532.

[2] a) C. W. Tang, *Appl. Phys. Lett.* **1986**, *48*, 183; b) B. Oregan, M. Gratzel, *Nature* **1991**, *353*, 737; c) J. H. Zhao, A. H. Wang, M. A. Green, F. Ferrazza, *Appl. Phys. Lett.* **1998**, *73*, 1991; d) M. S. Leite, R. L. Woo, J. N. Munday, W. D. Hong, S. Mesropian, D. C. Law, H. A. Atwater, *Appl. Phys. Lett.* **2013**, *102*, 033901; e) J. Wallentin, N. Anttu, D. Asoli, M. Huffman,

I. Aberg, M. H. Magnusson, G. Siefer, P. Fuss-Kailuweit, F. Dimroth, B. Witzigmann, H. Q. Xu, L. Samuelson, K. Deppert, M. T. Borgstrom, *Science* **2013**, *339*, 1057.
[3] R. Bertani, *Geothermics* **2012**, *41*, 1.
[4] a) C. B. Field, J. E. Campbell, D. B. Lobell, *Trends Ecol. Evol.* **2008**, *23*, 65; b) M. Hoogwijk, A. Faaija, R. van den Broek, G. Berndes, D. Gielen, W. Turkenburg, *Biomass Bioenergy* **2003**, *25*, 119.
[5] a) J. Scruggs, P. Jacob, *Science* **2009**, *323*, 1176; b) S. Chiba, M. Waki, R. Kornbluh, R. Pelnine, *Proc. SPIE* **2008**, *6927*, 692715.
[6] a) M. R. Islam, S. Mekhilef, R. Saidur, *Renew. Sust. Energy Rev.* **2013**, *21*, 456; b) R. D. Kornbluh, R. Pelrine, H. Prahlad, A. Wong-Foy, B. McCoy, S. Kim, J. Eckerle, T. Low, *Proc. SPIE* **2011**, *7976*, 797605.
[7] a) X. D. Wang, J. H. Song, J. Liu, Z. L. Wang, *Science* **2007**, *316*, 102; b) Y. Qin, X. D. Wang, Z. L. Wang, *Nature* **2008**, *451*, 809.
[8] a) P. D. Mitcheson, P. Miao, B. H. Stark, E. M. Yeatman, A. S. Holmes, T. C. Green, *Sens. Actuators A* **2004**, *115*, 523; b) R. Pelrine, R. Kornbluh, J. Eckerle, P. Jeuck, S. J. Oh, Q. B. Pei, S. Stanford, *Proc. SPIE* **2001**, *4329*, 148.
[9] a) T. von Buren, P. D. Mitcheson, T. C. Green, E. M. Yeatman, A. S. Holmes, G. Troster, *IEEE Sens. J.* **2006**, *6*, 28; b) S. P. Beeby, R. N. Torah, M. J. Tudor, P. Glynne-Jones, T. O'Donnell, C. R. Saha, S. Roy, *J. Micromech. Microeng.* **2007**, *17*, 1257.
[10] a) F. R. Fan, Z. Q. Tian, Z. L. Wang, *Nano Energy* **2012**, *1*, 328; b) G. Zhu, Z. H. Lin, Q. S. Jing, P. Bai, C. F. Pan, Y. Yang, Y. S. Zhou, Z. L. Wang, *Nano Lett.* **2013**, *13*, 847; c) G. Zhu, J. Chen, Y. Liu, P. Bai, Y. S. Zhou, Q. S. Jing, C. F. Pan, Z. L. Wang, *Nano Lett.* **2013**, *13*, 2282; d) Y. S. Zhou, Y. Liu, G. Zhu, Z. H. Lin, C. F. Pan, Q. S. Jing, Z. L. Wang, *Nano Lett.* **2013**, *13*, 2771.
[11] G. S. P. Castle, *J. Electrostat.* **1997**, *40–1*, 13.
[12] S. Wang, L. Lin, Z. L. Wang, *Nano Lett.* **2012**, *12*, 6339.
[13] P. Bai, G. Zhu, Z. H. Lin, Q. S. Jing, J. Chen, G. Zhang, J. Ma, Z. L. Wang, *ACS Nano* **2013**, *7*, 3713.
[14] A. F. Diaz, R. M. Felix-Navarro, *J. Electrostat.* **2004**, *62*, 277.
[15] S. H. Wang, L. Lin, Y. N. Xie, Q. S. Jing, S. M. Niu, Z. L. Wang, *Nano Lett.* **2013**, *13*, 2226.
[16] Z. L. Wang, *ACS Nano* **2013**, *7*, 9533.
[17] H. Fang, W. Z. Wu, J. H. Song, Z. L. Wang, *J. Phys. Chem. C* **2009**, *113*, 16571.
[18] J. C. Wilcke, *Disputatio Physica Experimentalis, De Electricitatibus Contrariis*, Rostochii: Typis Ioannis Iacobi Adleri, 1757.
[19] S. Niu, Y. Liu, S. Wang, L. Lin, Y. S. Zhou, Y. Hu, Z. L. Wang, *Adv. Mater.* **2013**, *25*, 6184.
[20] a) L. Lin, S. H. Wang, Y. N. Xie, Q. S. Jing, S. M. Niu, Y. F. Hu, Z. L. Wang, *Nano Lett.* **2013**, *13*, 2916; b) G. Zhu, Z.-H. Lin, Q. Jing, P. Bai, C. Pan, Y. Yang, Y. Zhou, Z. L. Wang, *Nano Lett.* **2013**, *13*, 847.